Analytical Methods

PAPER

View Article Online
View Journal | View Issue

Cite this: *Anal. Methods*, 2015, **7**, 2055

Thermoelectric lab-on-a-chip ELISA

Gergana G. Nestorova,[a] Varun L. Kopparthy,[a] Niel D. Crews[b] and Eric J. Guilbeau*[a]

Received 19th November 2014
Accepted 12th January 2015

DOI: 10.1039/c4ay02764g

www.rsc.org/methods

We report a new, thermoelectric method for performing enzyme-linked immunosorbent assay (ELISA) in a microfluidic device. The concentration of the analyte is determined by measuring the heat of an enzymatic reaction between glucose and glucose oxidase using thin-film antimony/bismuth thermopile. The feasibility of lab-on-a-chip thermoelectric ELISA is demonstrated by measuring the concentration of 8-hydroxy-2-deoxyguanosine (8OHdG) in urine samples from amyloid precursor protein transgenic mice. The detection method is based on formation of a complex between 8OHdG, anti-8OHdG capture antibody and glucose oxidase linked IgG antibody. The complex is immobilized at the lower channel wall of the microfluidic device, over the measuring junctions of the thermopile. The amount of heat detected by the thermoelectric sensor is inversely proportional to the concentration of 8OHdG. Standard calibration curve was created using synthetic 8OHdG. The regression line equation of the standard calibration curve was used to estimate the concentration of 8OHdG in mouse urine.

Introduction

ELISA is used as a diagnostic tool in medical research and as an analytical method for determining the concentration of antigens and antibodies in biomedical and environmental studies. The detection method is based on binding of an antigen and antibody followed by absorbance, fluorescent or luminescent detection of the chemical reaction between an enzyme-linked detection antibody and its substrate. The reporter antibody is conjugated to a suitable enzyme, such as horseradish peroxidase or alkaline phosphatase that generates luminescent signal or color change upon reaction with a substrate. The intensity of the signal is dependent on the concentration of the analyte.[1] Developments in the field of microfluidics and point of care diagnostics opened new avenues for performing ELISA in micro fabricated devices. The advantages of microfluidic ELISA are enhanced rate of reaction, shorter incubation times, reduced reagents cost and sample consumption coupled with accurate control of the fluid flow in the microchannel and reduced number of steps when compared to conventional ELISA.[2]

A variety of detection technologies have been employed in microfluidic ELISA systems that include fluorescence, chemiluminescence, and electrochemical detection. The product of the reaction between horseradish peroxidase (HPR) labeled antibody and 3-(*p*-hydroxyphenyl)-propionic acid (HPPA) has been measured using photon counting spectrofluorometer.[3] Complex photosensitive detectors were employed to detect the product of the enzymatic reaction between HRP labeled antibody and a substrate.[4] The pH change due to an enzymatic reaction between urease conjugated antibody and urea was detected using a semiconductor type of nanosensor.[5] An electrochemical microfluidic immunoassay has been developed to quantify the product of the reaction between HRP and 3,3′,5,5′-tetramethylbenzidine (TMB).[6] Enzyme mediated signal amplification using reduction of silver ions on gold nanoparticles was measured using photodetectors.[7] A camera cell phone was used to measure the levels of IgG when ELISA was performed using gold nanoparticles enhanced silver staining.[8] An inverted fluorescent microscope equipped with a digital monochrome camera was used to detect the fluorescent product of the enzymatic reaction between HRP and a substrate.[7] Thermal lenses have been successfully used to measure the levels of IgG.[9] Label-free ELISA was performed using surface plasmon resonance that senses in real-time the interactions between the antibody and the analyte.[10]

Thermoelectric lab-on-a-chip ELISA

We describe, thermoelectric method for performing ELISA (t-ELISA) in a microfluidic calorimeter with integrated thin-film thermopile. Previous work in the field of calorimetry includes application of thermistor to measure the heat of the enzymatic reaction between hydrogen peroxide and catalase for ELISA applications.[11] We demonstrate the feasibility of a microfluidic calorimeter with integrated thin-film thermopile to detect the heat of the reaction between an enzyme-conjugated antibody and a substrate for ELISA applications. Microfluidic calorimetry offers multiple advantages over standard calorimetry, including increased heat and mass transfer efficiencies, less sample volume, and faster response time. Applications of microfluidic calorimetry include, detecting the heat of the reaction between glucose and glucose oxidase,[12–14] urea and urease,[15] and sodium

[a]*The Center for Biomedical Engineering and Rehabilitation Science, Louisiana Tech University, USA. E-mail: ericg@latech.edu*

[b]*Institute for Micromanufacturing, Louisiana Tech University, USA*

hydroxide and sulfuric acid[16] using thermoelectric sensors. While previous work was focused on detection the heat of enzymatic reactions using thermoelectric platforms, we report a new method for performing ELISA that is based on measuring the thermoelectric signal caused by the reaction between glucose oxidase conjugated to a detection antibody and glucose. The microfluidic calorimeter does not require complex temperature control of ambient temperature and the temperature of the reference junction since thermal events common to both the reference and measuring junctions are rejected by the thermopile.[17] In thermoelectric ELISA, the concentration of the analyte is determined by detecting the heat of the enzymatic reaction between an enzyme-conjugated detection antibody and a substrate using a thin-film thermopile. The amount of heat released during the enzymatic reaction depends on the number of enzyme linked antibody complexes immobilized at the lower channel wall, in the area within the measuring junctions of the thermopile. As the concentration of the analyte increases, the magnitude of the thermoelectric signal decreases. A possible mechanism that explains these observations is that as the concentration of the analyte increases, steric hindrance between the analyte and the enzyme conjugated secondary antibody reduces both the efficiency of the reaction and the number of enzyme linked complexes immobilized to surface (Fig. 1a). The thermopile has the sensitivity and accuracy to respond accurately to different concentrations of enzyme and rates of the enzymatic reaction.

The feasibility of t-ELISA was demonstrated by measuring the levels of 8-hydroxy-2-deoxyguansoine (8OHdG) in the urine of amyloid precursor protein (APP) transgenic mice. 8OHdG is the most common form of reactive oxygen species induced lesion of the DNA molecule. When oxidation occurs, a hydroxyl group is added to the 8th position of the guanine molecule and the oxidized product, 8OHdG, is excised and excreted in the urine. Urinary level of 8OHdG is a biomarker of generalized oxidative stress and represents the average rate of oxidative damage in the body.[18] Increased levels of 8OHdG in the urine is linked to a number of diseases associated with aging such as lung, bladder, and prostate cancer, diabetes, and Alzheimer's disease.[19–23]

Levels of 8OHdG were measured in the urine of amyloid precursor protein transgenic mice using capillary electrophoresis with laser induced detection (CE-LIF). APP transgenic mice exhibit the pathology associated with Alzheimer's disease, are prone to oxidative stress, and have high levels of 8OHdG.[24]

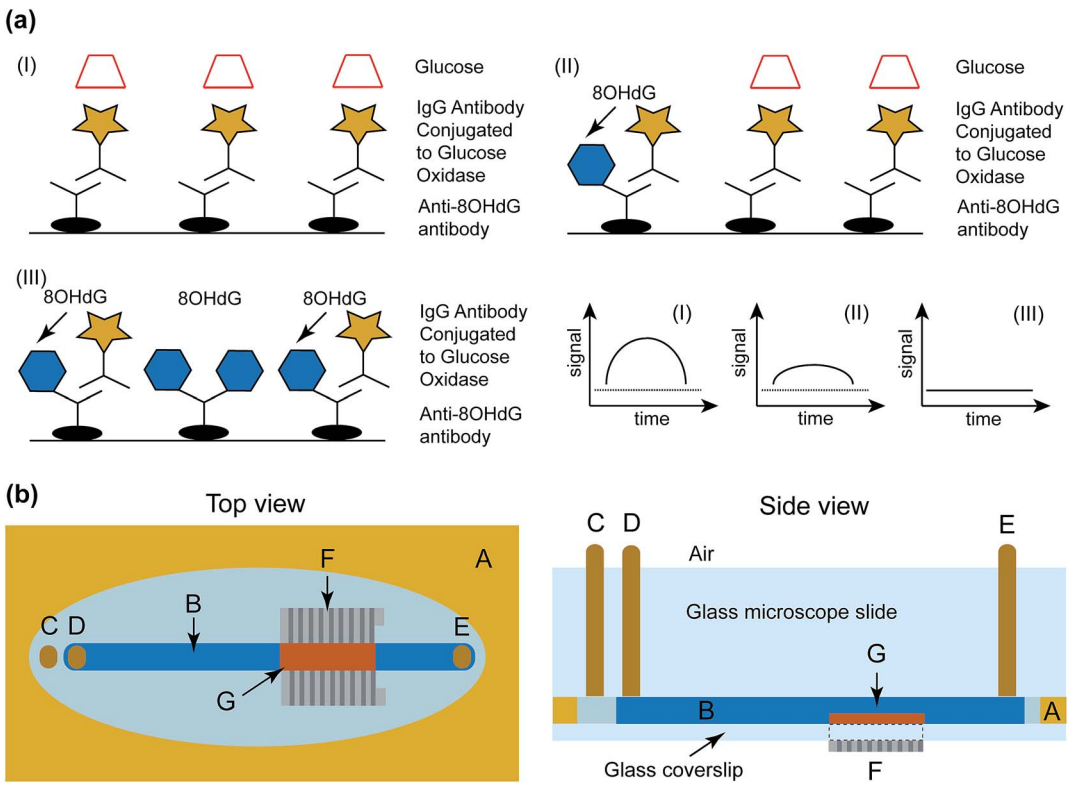

Fig. 1 (a) Thermoelectric method for performing ELISA. The concentration of the analyte is determined by detecting the heat of the enzymatic reaction between glucose oxidase that is conjugated to a detection antibody and glucose. The concentration of surface immobilized enzyme linked antibody complexes and the efficiency of the enzymatic reaction is inversely proportional to the concentration of the 8OHdG. (i) When the concentration of 8OHdG is 0 μm, the magnitude of thermopile signal response is high; (ii) and (iii), as the concentration of 8OHdG increases, the magnitude of sensor response decreases. (b) Schematic of microfluidic device with integrated thin-film thermopile. A is Kapton tape, that forms the channel wall, B is the hydrodynamically focused flow, C is inlet 1 that supplies the buffer solution that hydrodynamically constrains the glucose solution, D is inlet 2 that supplies glucose, E is outlet/waste, F is the thermopile, and G is the reaction zone, located at the lower channel wall of the microfluidic device.

Urinary level of 8OHdG reported using CE-LIF was compared with the results obtained using the thermoelectric ELISA.

Thermoelectric ELISA detection method is based on formation of a complex between 8OHdG, anti-8OHdG capture antibody conjugated to biotin, and glucose oxidase linked IgG antibody (IgG-GOD). The complex is immobilized to the streptavidin coated lower channel wall of a microfluidic device, in an area 3 mm × 6 mm, located directly over the measuring junctions of a thin-film thermopile. The microfluidic device consists of a 100 μm deep flow channel, two inlets, single outlet and thin-film antimony/bismuth (Sb/Bi) thermopile attached to the outer surface of the lower channel wall of the device using silver thermal compound. A 50 mM citrate/phosphate buffer, pH 5.3 is introduced through inlet 1 of the microfluidic device. Buffer solution containing glucose is introduced through inlet 2 of the microfluidic chip. The flow rate of the buffer being supplied through inlet 1 is 100 μL min^{-1}, while the flow rate of the buffer being supplied through inlet 2 is 25 μL min^{-1}. The width of the buffer introduced through inlet 2 is controlled by the relative flow rates of the both inlets and is hydrodynamically focused within the measuring junctions of the thermopile and the reaction zone.[25] The heat released during the oxidation of glucose is measured using a thin-film thermopile. The enzymatic reaction between glucose and glucose oxidase produces 79 kJ of heat per mole of glucose.[13]

$$\text{Glucose} + O_2 + H_2O \rightarrow \text{Gluconic acid} + H_2O_2 + 79\ \text{kJ mol}^{-1}$$

The temperature of the lower channel wall, under the reaction zone, increases when glucose is oxidized. The temperature change is detected by the measuring junctions of the thermopile but not by the reference junctions. The thermopile has a theoretical Seebeck coefficient of 7 μV mK^{-1} and excellent rejection of common mode thermal signals. The calorimeter was characterized by applying known quantities of energy to a nichrome heater incorporated on the inner side of the microfluidic sensor bottom channel wall, within the measuring junctions of the thermopile. Nichrome is an alloy of nickel, chromium, and iron that is used as a resistive heating element. The calculated Seebeck coefficient under experimental conditions was 7 μV mK^{-1} and the sensitivity of the device was estimated to be 0.045 V s J^{-1}.[26] The temperature difference between the measuring and the reference junctions of the thermopile causes change in the thermopile's electromotive force that is measured by a nanovoltmeter. Once the thermopile outputs returns to a baseline, the substrate can be introduced again to perform multiple measurements of the same sample that increases the statistical significance of the results.

Thermoelectric ELISA (t-ELISA) provides several advantages over traditional methods for performing enzyme-linked immunoassays. Conventional ELISA requires an expensive and bulky instrument equipped with absorbance, fluorescent or luminescent detectors. The assay is performed in a 96 well plate that requires large sample volume, longer incubation time due to the diffusion limitation of the reagents, and multiple pipetting steps. This prevents the application of ELISA in settings that require low cost and compact instrumentation.[27,28] Thermoelectric ELISA decreases the cost and complexity of the microplate reader by replacing absorbance, fluorescent, or luminescent detectors with a relatively inexpensive portable voltmeter and microfluidic chips with an integrated thermoelectric sensor. The cost of fabrication of the microfluidic device is reduced by employing xurography, a rapid prototyping fabrication technique that uses polyimide tape coated with adhesive.[29] In addition to reducing the cost and complexity of the instrument, performing thermoelectric ELISA in a microfluidic device decreases the cost of the reagents and the amount of sample that is used for the assay. Lab-on-a-chip t-ELISA decreases the time for the incubation steps by increasing the mass transfer rate of the analyte. Another advantage of the thermoelectric method is that it can be performed using a number of different enzymes because it is based on detection of the heat of the enzymatic reaction.

Heat transfer analysis

Steady-state mathematic model is developed to analyze the heat transfer from the reaction zone to the thermoelectric sensor. Schematic of the microfluidic calorimeter with integrated thin-film thermopile is shown in Fig. 1b. The microfluidic calorimeter is fabricated by attaching the thermopile beneath the outer surface of the lower channel wall. The reaction zone is located at the inner surface of the lower channel wall, within the measuring junctions of the thermopile. When enzymatic reaction occurs, heat is transferred from the coverslip to the thermopile and to the fluid that fills the channel (Fig. 2a). The total heat that is generated (Q) is given by eqn (1):

$$Q = q_1 + q_2 \quad (1)$$

q_1 is the heat that is transferred towards the thermopile, and q_2 is the heat that is transferred towards the fluid.

$$q_1 = (T_{(c.s.)} - T_\infty)/(R_{(c.s.)} + R_{(p.f.)} + R_{(conv,1)}) \quad (2)$$

$$q_2 = (T_{(c.s.)} - T_\infty)/(R_{(conv,2)} + R_{(conv,3)} + R_{(g.s.)} + R_{(conv,4)}) \quad (3)$$

$T_{(c.s.)}$ and T_∞ are the temperatures of the cover slip and the air, $R_{(conv,1)}$ and $R_{(conv,4)}$ are the convection thermal resistance associated with glass slide and air and polyimide film and air respectively. $R_{(c.s.)}$, $R_{(p.f.)}$, and $R_{(g.s.)}$ are the thermal resistance of cover slip, polyimide film, and glass slide. The following equation is used to calculate the thermal resistance:[30]

$$R = L/(kA) \quad (4)$$

L is the thickness of the layer (m), k is the thermal conductivity (Wm^{-1} K^{-1}), and A is the area of the reaction zone (m^2). The width of the hydrodynamically focused sample is 4 mm and the length of the thermopile is 6 mm. The total area of the reaction zone is 24 mm^2. According to eqn (4), thermal resistance of the glass cover slip is 7.6 KW^{-1}, the polyimide film is 33.6 KW^{-1}, and the glass slide is 43.4 KW^{-1}. Convective thermal resistances

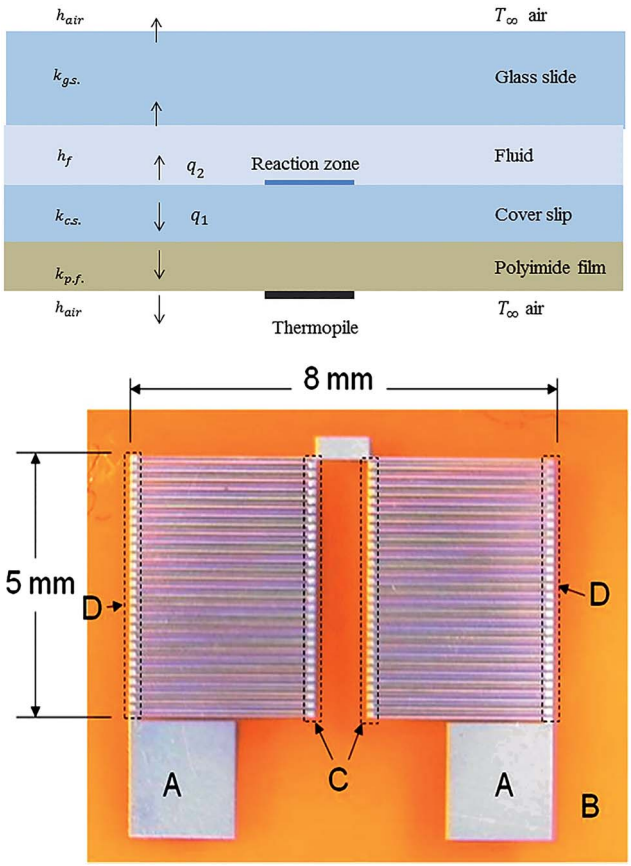

Fig. 2 (a) Heat transfer mathematical model of microfluidic calorimeter. $k_{(c.s.)}$, $k_{(p.f.)}$, and $k_{(g.s.)}$ are the conductive heat transfer coefficients of glass cover slip, polyimide film, and glass slide. $h_{(f)}$ and $h_{(air)}$ are the convective heat transfer coefficients at the interfaces between fluid and glass and fluid and air. (b) Antimony/bismuth thermopile with 60 thermocouple junctions (A = contact pads, B = polyimide support, C = measuring junctions, D = reference junctions).

between glass slide and air, coverslip and air, polyimide film and air, fluid and coverslip and fluid and glass are calculated according to the following equation:

$$R = 1/Ah \quad (5)$$

where h is the value of convective coefficient for air and fluid. The thermal resistance of air is 8333 KW^{-1}, and the thermal resistance of the fluid is 1.8 KW^{-1}. The thermal resistance towards the thermoelectric sensor is the cumulative thermal resistance of the glass cover slip, polyimide film and air, while the total thermal resistance towards the upper channel wall is the sum of the resistances of the fluid, glass slide, and air. The total thermal resistance towards the thermopile sensor is 8375 KW^{-1} and the total thermal resistance towards the glass slide is 8380 KW^{-1}. Based on the calculated values of thermal resistance coefficients, 50% of the heat generated by the enzymatic reaction is detected by the thermopile and 50% is transferred to the fluid and the upper channel wall.

We present a microfluidic system that measures heat of enzymatic reaction that occurs at the lower channel wall of the microfluidic device, at the interface of the fluid and the glass cover slip. Our thermopile's configuration results in rejection of common-mode thermal signals and has good stability when operated in laminar flow system.[17] Other reports in the literature include microfluidic calorimeters that measure heat of enzymatic reaction that occurs within the volume of the fluid being supplied *via* the inlets of the microfluidic device.[14] Under these experimental conditions the sensitivity of the calorimeter has to be improved significantly to account for the loss of heat in the fluid. The design of the thermoelectric sensor and the microfluidic chip described in this manuscript does not require complex control of the temperature simplifying the fabrication and operation of the calorimeter.

Experimental

Experimental overview

Thermoelectric detection and quantification of 8OHdG was performed using a microfluidic device with thin-film thermopile attached to the outer surface of the lower channel wall (Fig. 1b). The device contains a single flow channel that is 100 μm deep and 12 mm wide, two inlets and a single outlet. By adjusting the ratio of the flows through the two inlets of the microfluidic device, the glucose introduced through inlet 2 (25 μL min^{-1}) flows down the centerline of the device over the immobilized glucose oxidase linked antibody complex. The buffer introduced through inlet 1 (100 μL min^{-1}) flows only over the reference junctions of the thermopile. Laminar flow prevents the two fluid streams from mixing.[31]

A standard calibration curve was created by performing a dilution series using synthetic 8OHdG (0–10 μM). The standard calibration curve was used to estimate the concentration of 8OHdG in three urine samples from APP transgenic mice. The analyte, 8OHdG, was incubated with biotin conjugated anti-8OHdG antibody (6.5 μM). Primary antibody and 8OHdG complex was mixed with an IgG reporter antibody (6.5 μM) conjugated to glucose oxidase. Anti-8OHdG antibody/8OHdG/IgG-glucose oxidase antibody complex was immobilized at the lower channel wall of the microfluidic device, within the measuring junctions of the thermopile *via* biotin streptavidin interaction. The area within the measuring junctions of the thermopile was the reaction site. Glucose (55 mM), in 50 mM citrate/phosphate buffer was supplied *via* inlet 2 of the microfluidic device. The enzymatic reaction between glucose and glucose oxidase occurred at the surface of the lower channel wall within the measuring junctions of the thermopile. The heat of the enzymatic reaction between glucose and glucose oxidase was detected by a Sb/Bi thin-film thermopile.

Microfluidic device Manufacturing

The microfluidic chip consisted of two inlets and a single outlet (Fig. 1b). The lower channel wall consisted of a streptavidin coated glass cover slip. The upper channel wall consisted of a 25 mm × 75 mm microscope glass slide. The thickness of the glass slide was 1 mm and the thickness of the cover slip was 175 μm. Layer-by-layer self-assembly (LbL) was employed to form the

precursor layer for immobilizing of streptavidin on glass coverslips (Electron Microscopy Sciences, Hatfield, PA). Prior to the immobilization, the substrate was cleaned using 2% Micro-90 cleaning solution (Sigma Aldrich, St. Louis, MO). Poly-(ethylene imine) (PEI), (Sigma-Aldrich, Saint Louis, MO) and poly(acrylic acid) (PAcr), (Sigma Aldrich, Saint Louis MO) were used to form the precursor bilayers. A cleaned glass cover slip was immersed in PEI (50% w/v) and PAcr (35% w/v) alternatively for 15 minutes with intermediate rinsing and drying. PEI is a positively charged polyelectrolyte, while PAcr is a negatively charged one. This process was repeated to form three bilayers of alternating PEI/PAcr polyelectrolytes. The schematic of forming the bilayers was +/wash/−/wash/+/wash/−/wash/+/wash/−/wash. Biotin was attached to the PAcr polyelectrolyte layer *via* (1-[3-(dimethyl-amino) propyl]-3-ethylcarbodiimide hydrochloride) (EDC) linkage using biotin EZ link kit (Thermo Scientific, Rockford, IL). Amine-PEG-biotin was diluted in EDC buffer and pipetted onto the PAcr polyelectrolyte layer of the coverslip. The coverslip was placed in a humid chamber (37 °C, 90% humidity) for 30 minutes. The unreacted excess was washed with 10 mM MESb (pH 5.5) for two minutes followed by a wash with 10 mM Tris buffer (pH 7.5) for two minutes. Streptavidin was pipetted on the biotinylated polyelectrolyte multilayer placed in a humidity chamber for 30 minutes and washed with 10 mM Tris buffer.[32]

The microfluidic device was manufactured using xurography. A cutting plotter (Graphtec America Inc., Santa Ana, CA) was used to form the microfluidic channel out of 100 μm thick double sided Kapton® tape (3M, St. Paul, MN). The shape of the channel was designed using Adobe Illustrator (Adobe, San Jose, CA). The length of the channel was 62 mm, while the width was 12 mm. The Kapton® tape was sandwiched between a 25 mm × 75 mm plain glass microscope slide and a 25 mm × 75 mm streptavidin-coated glass coverslip. The thermopile was attached to the outer surface of the lower channel wall of the microfluidic device using silver thermal compound (Arctic Silver Inc., Visalia, CA).

Thermopile fabrication

Sb/Bi thermopiles with 60 thermocouple junction pairs were fabricated using a Denton model DV-502B metal evaporation system (Denton Vacuum, Moorestown, NJ) (Fig. 2b). Custom designed metal shadow masks containing the patterns for creating the thermopile's thin metal lines were designed using AutoCAD and manufactured by Town Technologies Inc. (Town Technologies Inc., Somerville, NJ). A rectangular piece of 125 μm thick polyimide tape (DuPont, Circleville, OH) was placed behind the shadow mask designed to create the bismuth line pattern and suspended above the evaporator heat source. Bismuth metal (Sigma-Aldrich Chemicals, St. Louis, MO) was heated until vaporized, and the vapors were allowed to condense on the support. The shadow mask containing the antimony line pattern was aligned to overlap with the bismuth lines at the thermocouple junctions. The evaporation process was repeated using antimony metal (Sigma-Aldrich Chemicals, St. Louis, MO). Following deposition of the antimony, the polyimide substrate with the thermopiles was removed from the chamber, tested for electrical continuity, and protected from physical damage using thin polyimide tape. The thermopile was attached to the streptavidin-coated coverslip using silver thermal compound (Arctic Silver Inc., Visalia, CA).

Thermoelectric ELISA measurement system

The microfluidic device with the thermopile attached to the lower channel wall was incorporated into a thermoelectric

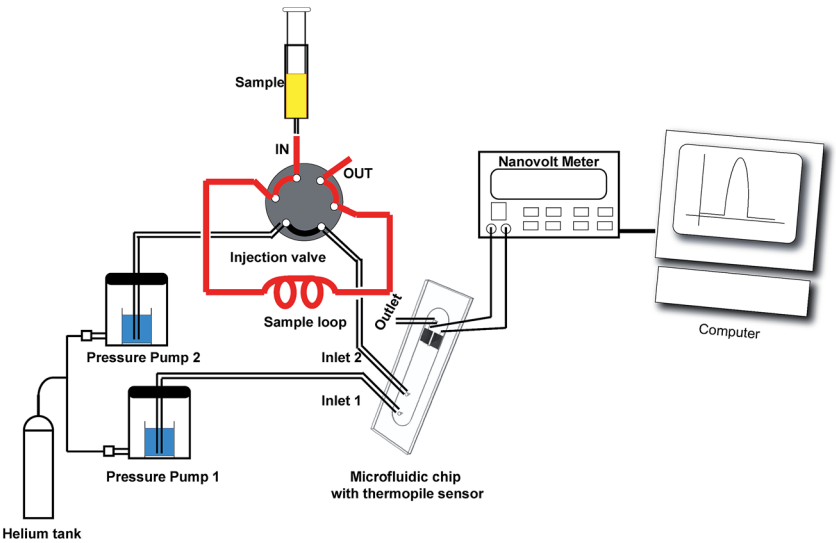

Fig. 3 Schematic of experimental set-up. Two pressure pumps provide independent injection of 50 mM phosphate/citrate buffer into inlet 1 and inlet 2 of the microfluidic device. Sample loop (52 μL) that is connected to an injection valve, is filled with glucose. Glucose is introduced in the buffer being supplied to inlet 2 through the injection valve. The enzymatic reaction between glucose and glucose oxidase occurs at the surface of the lower channel wall, directly over the measuring junctions of the thermopile. The voltage output of the thermopile is measured with nano voltmeter. The thermopile's signal is stored and displayed on computer using labview signalexpress software.

measurement system for ELISA analysis (Fig. 3). Two pressures driven Mitos P-Pumps (Dolmite Microfluidics, Charleston, MA) provided independent injection of 50 mM citrate/phosphate buffer, pH 5.3 through 254 μm internal diameter Teflon (ETFE) tubing (Upchurch Scientific, Oak Harbor, WA) into the inlet ports of the microfluidic device. A sample loop (52 μL) was filled with glucose (55 mM) in 50 mM citrate/phosphate buffer, pH 5.3 that was injected into the buffer stream being supplied to inlet 2 using a 6-Port Injection valve, (Model V-451, Upchurch Scientific, Oak Harbor, WA).

Standard calibration curve and quantification of 8OHdG in biological samples

Standard calibration curve was established by plotting the values of the signal that was integrated as function of time *versus* the concentration of the analyte. Serial dilutions were performed using stock standard of 10 μM 8OHdG (Sigma Aldrich Chemicals, St. Louis, MO). Area under the curve (AUC) of the thermopile signal for various concentrations of synthetic 8OHdG (0 μM, 2 μM, 3 μM, 6 μM and 10 μM) was calculated. The values for the AUC for each concentration of 8OHdG were calculated by averaging the results obtain using three microfluidic devices. Three injections of glucose were performed for each microfluidic device and the average value was calculated. The variation between and within experiments was calculated (Table 1 and 2).

Three μL of rabbit anti-8OHdG polyclonal antibody conjugated to biotin (6.5 μM) (Biossusa, Woburn, MA) were incubated with 2 μL 8OHdG (Sigma Aldrich, St. Louis, MO) for 30 minutes on an orbital shaker. Anti-rabbit IgG antibody (Abcam, Cambridge, MA) was conjugated to glucose oxidase using a glucose oxidase conjugation kit (Abcam, Cambridge, MA). Three μL of the secondary antibody (6.5 μM) was incubated with the mix of the primary antibody and 8OHdG for 30 minutes on an orbital shaker and immobilized to a streptavidin coated cover slip that formed the lower channel wall of the microfluidic device. The immobilization step was performed for 30 minutes at 37 °C in a humidity chamber, followed by a 2 min wash step with a 50 mM citrate/phosphate buffer. Fifty five μL of glucose (55 mM) was supplied *via* an injection valve connected to inlet 2 of the microfluidic device. The heat of the enzymatic reaction between glucose and glucose oxidase conjugated to the secondary antibody was detected using a thin-film Sb/Bi thermopile.

Table 1 AUC of the thermoelectric signal was calculated by performing three injections of glucose in the same device and averaging the values of the thermopile's response. Standard error represents the variation in the signal in the device

Concentration of 8OHdG	Average AUC of the signal	Standard error
0 μM	64.7 μV s	3.24
0 μM	46.4 μV s	14.86
0 μM	47.5 μV s	3.7
2 μM	32.63 μV s	0.82
2 μM	45.8 μV s	5.07
2 μM	43.53 μV s	1.49
3 μM	27.7 μV s	4.8
3 μM	28.5 μV s	9.7
3 μM	13.3 μV s	1
6 μM	15.2 μV s	2.4
6 μM	19.8 μV s	1.44
6 μM	19.75 μV s	3.34
10 μM	10.18 μV s	1.35
10 μM	16.87 μV s	2.05
10 μM	1.88 μV s	2.08

Table 2 Average AUC of the thermopile's response was calculated by averaging the values of the thermopile's response for three experiments. Standard error represents the variation in the signal between devices. Standard calibration curve was created by plotting the values for the concentration of 8OHdG *versus* the average AUC of the signal

Concentration of 8OHdG	Average AUC of the signal	Standard error
0 μM	52.86 μV s	5.93
2 μM	40.3 μV s	4.1
3 μM	23.12 μV s	4.94
6 μM	18.25 μV s	1.53
10 μM	9.64 μV s	4.34

Urine was collected from three APP transgenic mice according to the institutional guidelines. The urine collection protocol was reviewed and approved by the Louisiana Tech University Institutional Animal Care and Use Committee. The urine was centrifuged at 10 000 × *g* for two minutes to precipitate debris. The supernatant was collected and stored at −20 °C. Three μL of rabbit anti-8OHdG antibody conjugated to biotin (6.5 μM) was incubated with 2 μL of urine sample on an orbital shaker for 30 minutes. Three μL of secondary antibody (6.5 μM) conjugated to glucose oxidase was incubated with the complex of anti-8OHdG primary antibody and the urine sample on orbital shaker for 30 minutes. The complex was immobilized to a streptavidin cover slip. The coverslip was incorporated in a microfluidic device. The concentration of 8OHdG in the urine samples was calculated by performing three measurements of the enzymatic reaction and calculating the average AUC of the thermopile signal (Table 3). The regression line equation of the standard calibration curve was used to calculate the concentration of 8OHdG in the biological samples.

Data analysis

The voltage output of the thermopile was measured with Agilent 34420A nano voltmeter (Agilent, Santa Clara, CA). Voltmeter's measurements were recorded stored and displayed every second using LabView SignalExpress software (National Instruments, Austin, TX). The baseline drift of the signal was corrected using MatLab 7.5.0 (The MatLab Inc.) The amount of heat detected by the sensor was determined by calculating the area under the curve of the thermoelectric signal by integrating the area under the voltage *versus* time profile using the trapezoid rule. The AUC measurements were plotted *versus* the concentration of 8OHdG and the results were used to generate a standard curve. The regression line equation of the standard curve was used to calculate the concentration of 8OHdG in mouse urine samples.

Table 3 Average AUC of the signal was calculated using the values of the thermopile's response for three measurements of 8OHdG in mouse urine sample. Standard error represents variation of the signal between devices when biological sample was analyzed. The average AUC of the signal and the regression line equation of the standard calibration curve were used to calculate the concentration of 8OHdG

	Urine sample 1	Urine sample 2	Urine sample 3
AUC signal 1	30 μV s	40.9 μV s	22 μV s
AUC signal 2	44.8 μV s	56.2 μV s	35.4 μV s
AUC signal 3	32.6 μV s	16 μV s	25.2 μV s
Average AUC	35.8 μV s	37.7 μV s	27.53 μV s
Standard error	4.57	11.73	4.04
Concentration of 8OHdG	**2.05 μM**	**2.04 μM**	**4.52 μM**

Results

Standard calibration curve

The calibration curve was created by plotting the concentration of 8OHdG *versus* the average area under the curve of the thermoelectric signal corresponding to each concentration. The peak height of the thermoelectric signal increased from 100 nV to 600 nV as the concentration of 8OHdG decreased from 10 μM to 0 μM. In the absence of the analyte, the peak height of the sensor response was 100 nV. Control experiments were included to evaluate the specificity of the microfluidic calorimeter. 50 mM citrate/phosphate buffer, pH 5.3 was introduced in the microfluidic device *via* inlet 2. Thermoelectric response was not detected in the absence of glucose (Fig. 4a). The relationship between the concentration of the analyte and average AUC of the thermoelectric signal was described by the regression line equation. The correlation coefficient of the data points of the calibration curve was 0.8392 (Fig. 4b). The statistical variation in the measured signal within and between devices was calculated (Tables 1 and 2).

Urine sample analysis

The concentration of 8OHdG in urine samples obtained from three APP transgenic mice was measured using thermoelectric ELISA. Fig. 4c shows a thermoelectric signal that was detected when mouse urine sample was analyzed using t-ELISA. The drift in the thermoelectric signal was removed using a standard Matlab detrending algorithm. The duration of the signal was

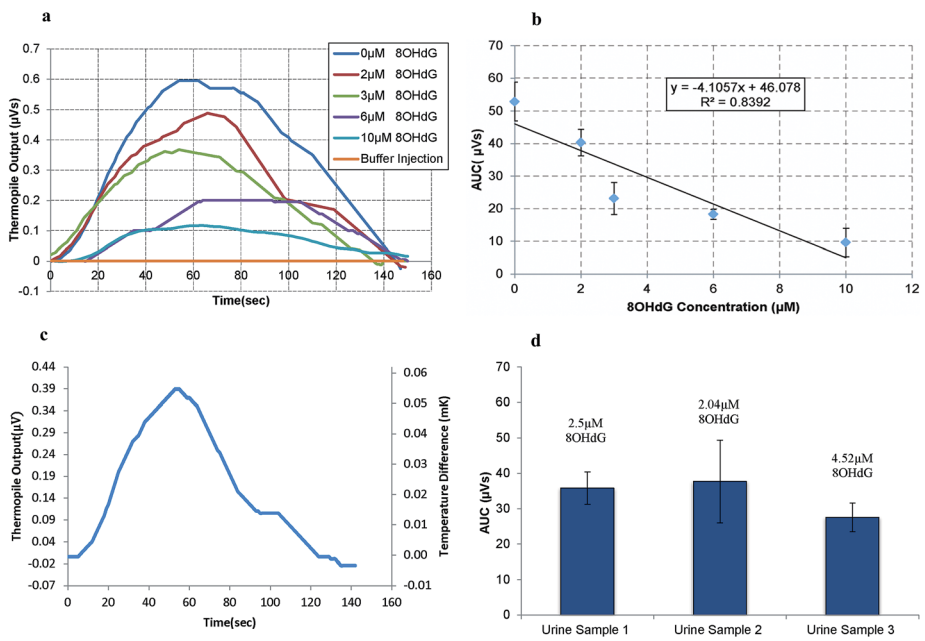

Fig. 4 Experimental results obtained using thermoelectric ELISA. (a) Thermoelectric signal, 10 μm, 6 μm, 3 μm, 2 μm, and 0 μm 8OHdG. Buffer injection represents the response of the thermopile when 50 mm phosphate/citrate buffer was introduced in the system. (b) Standard calibration curve, 0–10 μm 8OHdG. Area under the curve of the thermoelectric signal was plotted *versus* the concentration of synthetic 8OHdG. The standard error was calculated based on the values for the AUC of the thermoelectric response for three experiments. (c) Thermoelectric response when 8OHdG was measured in urine sample from APP transgenic mice. Thermopile output (μV) represents the peak height of the thermoelectric signal, while the temperature difference (mK) represents the thermal difference between the measuring and the reference junctions of the thermopile. (d) Concentration of 8OHdG in the urine of APP transgenic mice. The error bars are calculated using the values of the signal from three experiments.

120 seconds and the peak height of the signal was 400 nV. Experimental value of Seebeck coefficient of Sb/Bi thin-film thermopile is 7 μV mK^{-1}.[26] The value of the Seebeck coefficient was applied to calculate the thermal difference between the measuring and the reference junctions of the thermopile. Thermopile output of 400 nV corresponds to 0.05 mK temperature difference between the junctions of the sensor (Fig. 4c). Each urine sample was analyzed three times, and the concentration of 8OHdG was determined by calculating the average values of the AUC of the thermopile's response. The area under the curve and standard error for each experiment are presented in Table 3. The concentration of 8OHdG in each urine sample was respectively 2.5, 2.04, and 4.52 μM (Fig. 4d).

Discussion

The magnitude of the thermoelectric response is inversely proportional to the concentration of 8OHdG. The concentration of the surface immobilized enzyme and the efficiency of the enzymatic reaction have an effect on the slope, peak height and the area under the curve of the thermopile response (Fig. 4a). Negative control experiments were performed by introducing 50 mM citrate/phosphate buffer instead of glucose. These experiments confirmed that the magnitude of the signal is not affected by thermal events associated with introduction of the buffer in the microfluidic system.

The AUC of the thermoelectric response decreases as the concentration of 8OHdG increases. The regression line equation of the standard calibration curve shows that the upper limit of the AUC of the thermopile signal is 46.078 μV s. This value for the AUC corresponds to a 10 μM concentration of 8OHdG (Fig. 4b). There are two possible mechanisms that can explain the decrease of the thermoelectric response as the concentration of the analyte increases. Increased levels of 8OHdG could affect the efficiency of binding between the primary and the secondary antibody. As a result, the concentration of the surface immobilized enzyme is reduced. Another possible mechanism involves decreased efficiency of the enzymatic reaction as the concentration of the analyte increases. Higher levels of the analyte could interfere with the rate of the enzymatic reaction by physically obstructing the active sites of the enzyme.

The reproducibility of the measurements within and between experiments depends on several factors. Factors that add to the variation in the thermoelectric signal include the number of available streptavidin binding sites, the efficiency of the coupling reaction between the secondary antibody and glucose oxidase, the Seebeck coefficient of the thermopile, and the stability of the flow rates.

The reported level of 8OHdG in APP mouse urine sample, measured by capillary electrophoresis with lased induced detection (CE-LIF) was 1.82 μM.[24] The levels of 8OHdG measured using t-ELISA in three different urine samples from APP transgenic mice were 2.25 μM, 1.87 μM, and 3.94 μM (Fig. 4d). The quantification of 8OHdG using CE-LIF was performed on a single sample and does not reflect the variability in a sample population. Variation in the concentration of 8OHdG in the urine samples depends on the overall level of oxidative stress in the organism. The overall level of oxidative stress in APP transgenic mice is higher when compared to normal mice due to the mutation in the APP gene. The quantification of 8OHdG using lab-on-a-chip thermoelectric ELISA was performed using a polyclonal anti-8OHdG antibody, while the CE-LIF was performed using a monoclonal one. The polyclonal antibody has lower specificity for 8OHdG and it may cross react with other products of the oxidative stress repair pathway, such as the modified base or the modified 8-hydroxyguanosine that is the product of the RNA repair. This is an additional factor that accounts for the variation in the thermoelectric response when 8OHdG was measured in urine samples.

Future work will focus on development of methods for immobilizing a monoclonal antibody or analyte to the surface of the microfluidic device and evaluating thermoelectric ELISA by performing sandwiched, competitive and direct ELISA. Work will be performed to increase the sensitivity and decrease the response time of the system. This will include modifying the design of the thermoelectric sensor and the materials that are used for fabrication of the microfluidic device. The work will be extended to include applications of thermoelectric ELISA for pathogen detection as well as for detection of a variety of analytes and biomarkers.

Conclusion

We have developed thermoelectric microfluidic system that can be used for enzyme linked immunosorbent assay applications. The feasibility of a thermoelectric ELISA was demonstrated by measuring the concentration of 8OHdG in a microfluidic device. This method for detection of analytes has multiple applications including the areas of pathogen detection as well as for quantification of levels of environmental pollutants.

References

1 R. de La Rica and M. M. Stevens, *Nat. Nanotechnol.*, 2012, **7**, 821–824.
2 C. A. Baker, C. T. Duong, A. Grimley and M. G. Roper, *Bioanalysis*, 2009, **1**, 967–975.
3 E. Eteshola and D. Leckband, *Sens. Actuators, B*, 2001, **72**, 129–133.
4 P. Novo, D. M. F. A. Prazeres, V. Chu and J. O. P. Conde, *Lab Chip*, 2011, **11**, 4063–4071.
5 E. Stern, A. Vacic, C. Li, F. N. Ishikawa, C. Zhou, M. A. Reed and T. M. Fahmy, *Small*, 2010, **6**, 232–238.
6 M. H. Shamsi, K. Choi, A. H. Ng and A. R. Wheeler, *Lab Chip*, 2014, **14**, 547–554.
7 C. D. Chin, T. Laksanasopin, Y. K. Cheung, D. Steinmiller, V. Linder, H. Parsa, J. Wang, H. Moore, R. Rouse and G. Umviligihozo, *Nat. Med.*, 2011, **17**, 1015–1019.
8 Y. Lu, W. Shi, J. Qin and B. Lin, *Electrophoresis*, 2009, **30**, 579–582.
9 T. G. Henares, S.-I. Funano, S. Terabe, F. Mizutani, R. Sekizawa and H. Hisamoto, *Anal. Chim. Acta*, 2007, **589**, 173–179.

10 K.-H. Lee, Y.-D. Su, S.-J. Chen, F.-G. Tseng and G.-B. Lee, *Biosens. Bioelectron.*, 2007, **23**, 466–472.
11 B. Mattiasson, C. Borrebaeck, B. Sanfridson and K. Mosbach, *Biochim. Biophys. Acta*, 1977, **483**, 221–227.
12 B. Davaji and C. H. Lee, *Biosens. Bioelectron.*, 2014, **59**, 120–126.
13 S. M. Tangutooru, V. L. Kopparthy, G. G. Nestorova and E. J. Guilbeau, *Sens. Actuators, B*, 2012, **166**, 637–641.
14 J. Lerchner, A. Wolf, G. Wolf, V. Baier, E. Kessler, M. Nietzsch and M. Krügel, *Thermochim. Acta*, 2006, **445**, 144–150.
15 W. Lee, W. Fon, B. W. Axelrod and M. L. Roukes, *Proc. Natl. Acad. Sci.*, 2009, **106**, 15225–15230.
16 J. M. Köhler and M. Zieren, *Thermochim. Acta*, 1998, **310**, 25–35.
17 G. G. Nestorova and E. J. Guilbeau, *Lab Chip*, 2010, **11**, 1761–1769.
18 L. L. Wu, C.-C. Chiou, P.-Y. Chang and J. T. Wu, *Clin. Chim. Acta*, 2004, **339**, 1–9.
19 S. Loft, P. Svoboda, H. Kasai, A. Tjønneland, U. Vogel, P. Møller, K. Overvad and O. Raaschou-Nielsen, *Carcinogenesis*, 2006, **27**, 1245–1250.
20 M. Erhola, S. Toyokuni, K. Okada, T. Tanaka, H. Hiai, H. Ochi, K. Uchida, T. Osawa, M. M. Nieminen and H. Alho, *FEBS Lett.*, 1997, **409**, 287–291.
21 C. C. Chiou, P. Y. Chang, E.-C. Chan, T.-L. Wu, K.-C. Tsao and J. T. Wu, *Clin. Chim. Acta*, 2003, **334**, 87–94.
22 H. Pan, D. Chang, L. Feng, F. Xu, H. Kuang and M. Lu, *Biomed. Environ. Sci.*, 2007, **20**, 160.
23 A. Nunomura, G. Perry, G. Aliev, K. Hirai, A. Takeda, E. K. Balraj, P. K. Jones, H. Ghanbari, T. Wataya and S. Shimohama, *J. Neuropathol. Exp. Neurol.*, 2001, **60**, 759–767.
24 C. Zhang, G. Nestorova, R. A. Rissman and J. Feng, *Electrophoresis*, 2013, **34**, 2268–2274.
25 G.-B. Lee, C.-C. Chang, S.-B. Huang and R.-J. Yang, *J. Micromech. Microeng.*, 2006, **16**, 1024.
26 V. L. Kopparthy, S. M. Tangutooru, G. G. Nestorova and E. J. Guilbeau, *Sens. Actuators, B*, 2012, **166–167**, 608–615.
27 S. K. Sia, V. Linder, B. A. Parviz, A. Siegel and G. M. Whitesides, *Angew. Chem., Int. Ed.*, 2004, **43**, 498–502.
28 R. Hawkes, E. Niday and J. Gordon, *Anal. Biochem.*, 1982, **119**, 142–147.
29 D. A. Bartholomeusz, R. W. Boutte and J. D. Andrade, *J. Microelectromech. Syst.*, 2005, **14**, 1364–1374.
30 F. Incropera and D. DeWitt, *Fundamentals of Heat and Mass Transfer*, 2001, 5th edn.
31 D. Lee, C. Chang, S. Huang and R. Yang, *J. Micromech. Microeng.*, 2006, 1024–1032.
32 E. P. Kartalov, M. A. Unger and S. R. Quake, *Biotechniques*, 2003, **34**, 505–510.